PERGAMON

International Journal of Heat and Mass Transfer 44 (2001) 195–206

International Journal of HEAT and MASS TRANSFER

www.elsevier.com/locate/ijhmt

Numerical investigation of bubble growth and detachment by the lattice-Boltzmann method

Z.L. Yang*, T.N. Dinh, R.R. Nourgaliev, B.R. Sehgal

Division of Nuclear Power Safety, Royal Institute of Technology, Drottning Kristinas vag 33, 10044 Stockholm, Sweden

Received 27 January 1999; received in revised form 14 January 2000

Abstract

A numerical study has been performed to investigate the characteristics of bubble growth on, and detachment from, an orifice. The FlowLab code, which is based on a lattice-Boltzmann model of two-phase flows, was employed. Macroscopic properties, such as surface tension (σ) and contact angle (β), were implemented through the fluid–fluid (G_σ) and fluid–solid (G_t) interaction potentials. The model was found to possess a linear relation between the macroscopic properties (σ, β) and microscopic parameters (G_σ, G_t). The separate effects of the body force (gravity), gas injection rate, surface tension, and wettability were analyzed for both horizontal and vertical surfaces. It is shown that results of the lattice-Boltzmann modeling exhibit correct parametric dependencies of the departure diameter of bubbles generated on the horizontal surface on the above factors as previously established in experiments. For the case of bubble growth and departure on the vertical surface, the different effects of hydrodynamic parameters, except gas generation rate, were predicted.

1. Introduction

Bubble dispersions in liquids play an important role in the development of various contacting devices used in power and chemical engineering industries. Bubble dispersions are most commonly produced by blowing a gas into a liquid through either perforated plates or nozzle grids. To enable description of the bubble dispersion phenomena, it is instructive to understand the underlying physical mechanisms that govern the bubble formation on a single orifice or nozzle. This has been a topic of numerous experimental studies conducted at normal gravity. Theoretical models were also developed to explain results from experiments in which gas was injected into both viscous and inviscid fluids. All of these models presume buoyancy to be the primary factor that ultimately causes the bubbles to detach themselves.

Under normal conditions, there are three known bubbling regimes at a submerged plate orifice. These are the static, the turbulent, and the dynamic regimes [1]. The static regime occurs at very low gas flow rates when both inertial and viscous forces may be overlooked. In the static regime, the moment of detachment, and the final bubble volume, are determined by a limiting equilibrium configuration of the gas cavity based on the orifice rim. This limiting configuration is established under the combined action of surface tension and gravity forces. Bubble detachment volume in this static regime is independent of gas flow rate, whereas bubble detachment frequency is proportional to gas flow rate [2,3].

The turbulent regime, in contrast, occurs at very

* Corresponding author.

0017-9310/01/$ - see front matter
PII: S0017-9310(00)00101-0

Nomenclature

D	bubble diameter, m
e, c	lattice speed, m/s
f, n	distribution function
F	force, N
G	interaction strength
g	gravity acceleration, m/s^2
m	molecular weight of component
n	particle distribution
P	pressure, N/m^2
Q	flow rate, m^3/s
t	time, s
u	velocity, m/s
v	gas velocity, m/s
x	coordinates (x, y), m

Greek symbols

β	contact angle, degree
ν	kinematic viscosity, m^2/s
ρ	density, kg/m^3
τ	relaxation time
ψ	effective number density
σ	surface tension, N/m

Subscripts/superscripts

a	index of discrete lattice velocity
b	number of the discrete velocities
c	critical value
eq	equilibrium
g	gravity
S	number of phases
σ	index of phase, surface tension
t	fluid–solid interaction

high flow rates when successively emerged bubbles coalesce close to the orifice, and after that they disintegrate into smaller bubbles of varying sizes and irregular shapes and hence participate in a vigorous swirling motion. Such bubbles cannot certainly be treated as separate independent entities, and this explains why there is seemingly no reliable model of the turbulent boiling regime [4].

The dynamic regime is characteristic of systems using an intermediate range of gas flow rates, that is, flow rates which are most often used in industrial applications. This range extends as high as gas flow rates of the order of 10^4 cm^3/s for air–water systems [5]. The main feature of the dynamic regime is that its bubbles may be considered more or less independent of one another. Of course, the concept of a single growing bubble in this regime is somewhat of an idealization, since distinction must be made between different subregimes, such as those of single and double bubbling, single and double pairing and delayed release (see e.g., Ref. [1] for a comprehensive review). Bubble evolution is governed by the inertial, viscous, surface tension and buoyancy forces. Except for cases when gas is injected into highly viscous Newtonian and non-Newtonian liquids, viscous forces happen to be small in comparison to the inertial and buoyancy forces. For the dynamic regime, the liquid may effectively be regarded as inviscid, as in many practical situations.

Numerous experimental and theoretical studies have been performed on the bubble formation and detachment on the horizontal surface. Almost all existing models of bubble growth and detachment in gas-injected systems, including the pioneering works [6–8] and the two-stage model developed later in [5], assume that a growing bubble remains spherical throughout the entire period of its evolution and at detachment, the fluid (liquid), ideally, wets the solid materials. Though these models correlated well with experimental observations, confirming the plausibility of the basic assumptions, the small variation range of experimental parameters, e.g., normal gravity and ideal wetting characteristics of fluid–solid contact, limit the applications of these models, especially, for cases with low gravity and for fluids of different wettability.

Very few studies have been reported regarding the single bubble behavior on the vertical surface. In particular, the interaction between bubbles makes the experimental measurement difficult, and the irregular shape of bubble detached from a vertical surface largely complicates theoretical analyses. As a result, no comprehensive physical and mathematical model describing characteristics of bubble growth and detachment on the vertical surface has been developed and validated.

The lattice-Boltzmann flow-modeling approach, which has been recently developed [9], recovers the Navier-Stokes equations in the incompressible flow limit. Since the lattice-Boltzmann method can be considered as a mesoscopic approach, lying between microscopic molecular dynamics and conventional macroscopic fluid dynamics, this method has been found very useful in problems involving surface tension, capillarity and phase transition in multiphase multicomponent systems [10].

In this work, the lattice-Boltzmann code FlowLab, developed at the Division of Nuclear Power Safety, Royal Institute of Technology [11], is employed for simulation of bubble formation and detachment under different conditions. The static and the dynamic bubbly regimes are investigated. The effects of gravity, surface tension, inertial force and wettability on bubble detachment size are analyzed. Since present capability of the lattice-Boltzmann modeling in the FlowLab code is limited to isothermal cases, we consider no change of phase and related mass transfer in the present study.

2. Formulation of the lattice-Boltzmann method

2.1. Basics of the lattice-Boltzmann method

The idea of the lattice-Boltzmann approach originates from the kinetic theory of gases, according to which, the dynamics of flow is described by an integro-differential Boltzmann equation:

$$\frac{\partial f}{\partial t} + \mathbf{u}\cdot\nabla f = \sum(\mathbf{x}, \mathbf{u}, t) \tag{1}$$

where $f(\mathbf{x}, \mathbf{u}, t)$ is the density distribution function, which represents a density of particles inside an infinitesimal phase space volume, $\Delta\Xi = \Delta x_i \Delta u_i$, of 6D phase space ($u_i$, x_i, $i = 1, 3$). The right-hand side of the Boltzmann equation (1) is a collision integral, which describes the source/sink of particles (due to collision) in the infinitesimal volume $\Delta\Xi$. The simplest model for the collision integral, which is valid in the case of small deviation of system from the equilibrium state, has the following form:

$$\sum(\mathbf{x}, \mathbf{u}, t) = -\frac{1}{\tau}\left(f - f^{\,\mathrm{eq}}\right) \tag{2}$$

where τ is the relaxation (towards equilibrium) time.

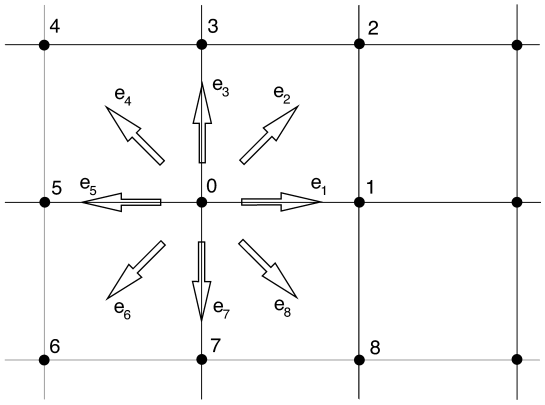

Fig. 1. Lattice geometry and velocity vectors of D2Q9 model.

The discrete-velocity-Boltzmann equation for multi-component and multiphase flow is derived from Eq. (1) [12]:

$$n_a^\sigma(\mathbf{x} + \mathbf{e}_a, t+1) - n_a^\sigma(\mathbf{x}, t) = -\frac{1}{\tau_\sigma}\left[n_a^\sigma(\mathbf{x}, t) - n_a^{\sigma(\mathrm{eq})}(\mathbf{x}, t)\right] \tag{3}$$

where $n_a^{\sigma(\mathrm{eq})}(\mathbf{x}, t)$ is the equilibrium distribution at ($\boldsymbol{x}$, t). Superscript σ denotes the fluid component, $\sigma = 1, \ldots, S$ and subscript a denotes the lattice velocity direction, $a = 1, \ldots, b$. It is instructive to note, that Eq. (3) is normalized by the lattice spacing, Δx, and the reference lattice speed, $c = \Delta x/\Delta t$.

The functional form for the equilibrium distribution of a rectangular two-dimensional nine-speed (D2Q9) model, shown in Fig. 1, is chosen as

$$n_0^{\sigma(\mathrm{eq})}(\mathbf{x}) = t_0 n^\sigma(\mathbf{x})\cdot\left[1 - \frac{3}{2}\mathbf{u}^2\right] \tag{4}$$

$$n_a^{\sigma(\mathrm{eq})}(\boldsymbol{x}) = t_i n^\sigma(\boldsymbol{x})\cdot\left[1 + 3\boldsymbol{e}_a\cdot\boldsymbol{u} + \frac{3}{2}\left(3\boldsymbol{e}_a\boldsymbol{e}_a{:}\boldsymbol{u}\boldsymbol{u} - \boldsymbol{u}^2\right)\right] \tag{5}$$

where $n^\sigma = \sum_{a=1}^{b} n_a^\sigma$, $t_0 = \frac{4}{9}$ (the rest population), $t_1 = \frac{1}{9}$ (population moving in diagonal directions) and $t_2 = \frac{1}{36}$ (population moving in non-diagonal directions). In the above expressions, arbitrary constant d_0 was chosen as 1/3 [14].

Physical quantities of flow, such as fluid density $\rho^\sigma(\mathbf{x}, t)$ and fluid velocity $\mathbf{u}^\sigma$, can be obtained from:

$$\rho^\sigma(\mathbf{x}, t) = \sum_a m^\sigma n_a^\sigma(\mathbf{x}, t) \tag{6}$$

$$\rho^\sigma(\mathbf{x}, t)\mathbf{u}^\sigma(\mathbf{x}, t) = \sum_\sigma m^\sigma \sum_a n_a^\sigma(\mathbf{x}, t)\mathbf{e}_a + \sum_a \mathbf{F}_a^\sigma \tag{7}$$

where m^σ is the molecular mass of the σth component, $\sum_a \mathbf{F}_a^\sigma$ is the momentum contributed by total forces acting on the σth component:

$$\sum_a \mathbf{F}_a^\sigma = \mathbf{F}_{\mathrm{g}}^\sigma + \mathbf{F}_\sigma^\sigma + \mathbf{F}_{\mathrm{t}}^\sigma \tag{8}$$

where $\mathbf{F}_g^\sigma$, $\mathbf{F}_\sigma^\sigma$ and $\mathbf{F}_{\mathrm{t}}^\sigma$ are momenta contributed by gravity, interaction between phases, and interaction of fluid with solid, respectively.

It was theoretically shown by Shan and Chen [12] that the lattice-Boltzmann formulation, described above, is an adequate model of macroscopic flow of an ideal fluid.

2.1.1. Interaction potential

In the present work, the interaction potential model

of Shan and Chen [12], which simulates the hydrodynamic interaction between two phases, is employed.

$$\mathbf{F}_{\sigma}^{\sigma} = -\tau_{\sigma}\psi^{\sigma}\sum_{\sigma'}^{S} G_{\sigma\sigma'}\sum_{a=0}^{b}\psi^{\sigma'}(\mathbf{x}+\mathbf{e}_a)\mathbf{e}_a \tag{9}$$

where ψ^{σ} is a function of $n(\mathbf{x})$ and plays the role of the effective number density for component σ. $G_{\sigma\sigma'}$ is the interaction potential. Only short-range interactions are represented in this model.

As shown in [13], with the above definition of the interaction potential, the equation of state for D2Q9 lattice-Boltzmann model can be written as

$$P = \frac{1}{2}\left[\sum_{\sigma}\frac{2}{3}\rho^{\sigma} + \frac{9}{2}\sum_{\sigma\sigma'}G_{\sigma\sigma'}\psi^{\sigma}\psi^{\sigma'}\right] \tag{10}$$

where the first term on the right-hand side is a kinetic contribution, while the second term is a contribution due to the inter-particle interaction. With interaction potential properly chosen, any equation of state can be modeled [13].

2.1.2. Fluid–solid interaction

The model, developed by Martys and Chen [14] to describe the interaction between a fluid and a wall, is implemented in the FlowLab code:

$$\mathbf{F}_{\mathrm{t}}^{\sigma} = -\tau_{\sigma}n^{\sigma}(\mathbf{x})\sum_{a}G_{\mathrm{t}}^{\sigma}s(\mathbf{x}+\mathbf{e}_a)(\mathbf{e}_a) \tag{11}$$

where G_{t}^{σ} is the fluid–solid interaction potential parameter, $s = 0$ or 1 for fluid or solid, respectively. By adjusting the interaction strength G_{t}^{σ} (positive for non-wetting fluid and negative for wetting fluid) for each pair of fluid–solid interaction, we control the surface wetting characteristic.

Applying the Chapman–Enskog expansion procedure to the lattice-Boltzmann equation(3), one obtains the following mass and momentum equations for the fluid mixture treated as a single fluid [13]:

$$\frac{\partial\rho}{\partial t} + \nabla\rho\mathbf{u} = 0 \tag{12}$$

$$\frac{\partial\mathbf{u}}{\partial t} + \mathbf{u}\nabla\mathbf{u} = -\frac{\nabla P}{\rho} + \frac{\sum_{a}\mathbf{F}_{a}^{\sigma}}{\rho} + \nu\nabla^{2}\mathbf{u} \tag{13}$$

where $\rho = \sum_{\sigma=1}^{S}\rho\sigma$ is the total density of the fluid mixture, $x^{j} = \rho^{j}/\rho$ is the mass fraction of the component j.

In the lattice-Boltzmann method, only fluid density is introduced directly. The kinematic viscosity of fluid can be obtained from,

$$\nu = \frac{2\tau - 1}{6} \tag{14}$$

where τ is the relaxation time in the lattice-Boltzmann equation. By choosing proper τ, the viscosity of fluid can be obtained.

2.2. Performance of the lattice-Boltzmann method for two-phase flow simulation

2.2.1. Boundary and initial conditions

It is easy to implement boundary conditions for the lattice-Boltzmann method. Typically, in order to reproduce no-slip boundary conditions, populations of particles are reflected along their directions ('bounce-back' conditions) in the lattice nodes, next to the boundary. Exact position of the wall is unknown, but it is usually set up to be in the middle of the boundary nodes and their neighbors. One may also define specular reflection conditions that yield a slip condition. The simplicity of such a formulation of boundary conditions makes the lattice-Boltzmann method very attractive for simulation of flow with complex boundaries.

By employing such boundary and initial conditions, since the lattice-Boltzmann equation (3) is explicit, the lattice-Boltzmann method is found to be very stable in the case that the March number of fluids is less than 1 and the relaxation time is larger than 0.5. It is confirmed that the lattice-Boltzmann method has second order of accuracy [15].

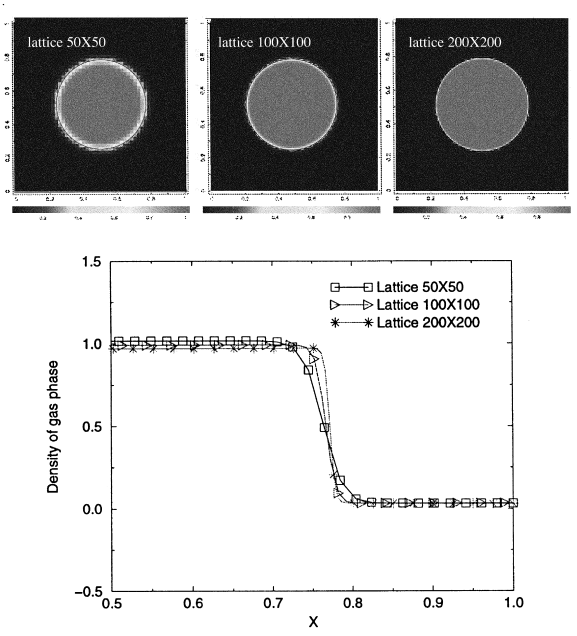

Fig. 2. Effect of the nodalization on the density distribution of gas phase across the interface, $G = 0.05$.

2.2.2. Capability to simulate complex topology of two-phase interfaces

In order to demonstrate the capability of the lattice-Boltzmann method to capture interface of two-phase flow, Shan and Chen [12] showed analytically that for a case with $\tau_\sigma = \tau$ the spin diffusivity, η, is negative, when $G_{\sigma\sigma'} > (\tau - 1/2)S/6$, which indicates a separation of components. Sehgal [11] performed a test of agglomeration of two immiscible fluids on 50×50 lattice with $\tau = 1$, $\rho_1/\rho_2 = 4/6$ and $G = 0.5 > G_c = 1/24$ [12]. Calculated results on the history of the component's separation in [11] show that the lattice-Boltzmann method has remarkable capability to simulate very complex topology of interfaces in dynamics without any special treatment of the interfaces.

In the present paper, a test on the sharpness of interface of two immiscible fluids in a physical domain with a scale of 1×1 and a static bubble size of 0.6 in radius is performed. Three different lattice (grid) representations, namely 50×50, 100×100 and 200×200, are employed. The simulation results are shown in Fig. 2. The upper pictures in Fig. 2 are the contours of density distribution of gas phase in the whole calculated domain, and the lower one shows the density distributions of gas phase along the central line in horizontal direction (X direction) starting from the center point of the static bubble to the right boundary of the calculated domain (see the upper picture of Fig. 2). It can be seen that the interface becomes sharper as the lattice number increases. Notably, the density change across the interface can be captured within three lattices.

2.2.3. Evaluation of surface tension

The surface tension of fluid in two-phase flow can be evaluated from the interaction potential G_σ [12]. In the present work, two-dimensional circular bubbles are generated in the center of the computational domain. For specific model parameters chosen (τ_σ, ρ^σ and G_σ), the fluid surface tension is calculated as a slope of $\Delta P \propto 1/R$ dependence. Fig. 3 presents a 'measurement' of the surface tension. As it shows, the Laplace law is represented quite well by the lattice-Boltzmann method.

Fig. 4 shows the simulation results of surface tension for different interaction potential parameters by the lattice-Boltzmann method. In the calculation, the lattice number is 51×51. The dependence of surface tension on the interaction potential G_σ is predicted nearly linear in this model ($\sigma \sim G_\sigma$).

2.2.4. Evaluation of contact angle

The contact angle of bubble interface on a solid surface depends not only on the fluid properties, but also on the fluid–solid interaction. In a previous work [10], it has been shown that the static contact angle β of two phases in the pool can be reasonably well predicted by Eq. (11) [14]. By measuring the contact angle β in the density distribution figure, obtained from the lattice-Boltzmann simulation with the 41×81 lattice, it is found in the present work that the static contact angle β is an inverse linear function of the fluid–solid interaction parameter G_t (Fig. 5). In this case, densities and the relaxation time are set to 1 for both fluids. For $G_t = 0$, the solid surface is totally wettable by both fluids. In contrast, a zero contact angle indicates that the solid surface becomes unwettable by one of the fluids. In general, a bigger contact angle is predicted for the fluid with larger surface tension coefficient ($\sigma \sim G_\sigma$); see Fig. 5. Successful applications of the FlowLab code and model to two-phase flows, while

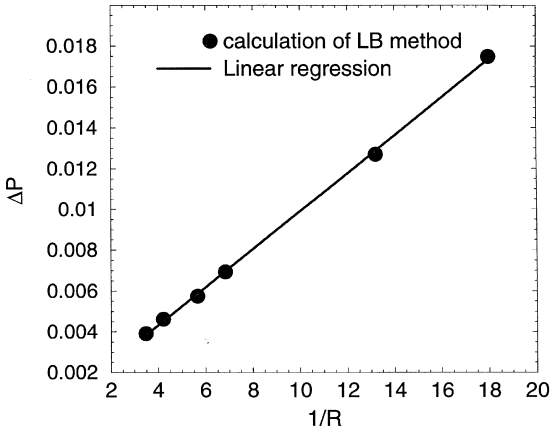

Fig. 3. Total pressure difference inside and outside of a circular bubble as a function of its curvature. The slope is the surface tension, $\tau_\sigma = 1$, $\rho^\sigma = 1$, $G_\sigma = 0.05$ and 100×100 lattice.

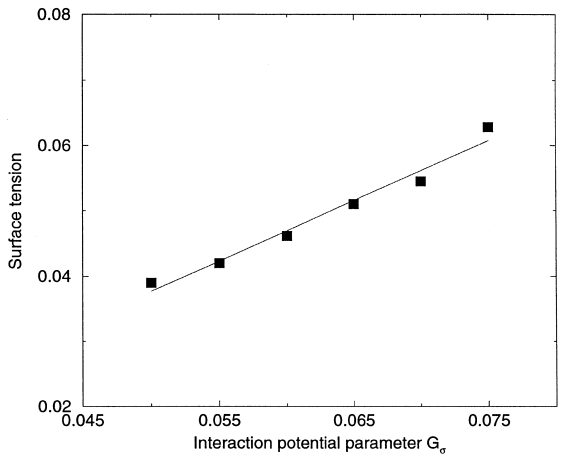

Fig. 4. Evaluation of surface tension for two-phase flow.

accounting for surface tension and wettability, were reported in Refs. [10,11].

3. Bubble growth and detachment on the horizontal surface

Generally, when a bubble forms at the horizontal solid surface, its growth characteristics and the moment of detachment depend on both liquid–solid interface condition (wettability effect) and the balance of forces, which include gravity (body force), surface tension, and inertial force of gas injection.

The most widely used correlation for the departure diameter D_d of bubble on the horizontal surface is that by Fritz [16] in which the bubble departure was determined by a balance between the buoyancy and surface tension forces acting normal to the solid surface:

$$D_d = 0.0208\beta\left(\frac{\sigma}{g\Delta\rho}\right)^{1/2} \tag{15}$$

Here, β is the contact angle in degrees, σ is surface tension coefficient, g is the gravity acceleration, $\Delta\rho$ is the density difference of two phases. Staniszewski [17] measured the departure diameter over a range of pressures and observed an influence of the bubble growth rate on the departure diameter. He modified the Fritz equation to obtain the departure diameter correlation,

$$D_d = 0.0071\beta\left(\frac{2\sigma}{g\Delta\rho}\right)^{1/2}\left(1 + 34.3\frac{\partial D}{\partial t}\right) \tag{16}$$

where $\partial D/\partial t$ is the bubble growth rate, which increases with the gas flow rate Q.

In the present work, gas is injected into a two-dimensional liquid pool through a nozzle from the pool bottom. The lattice-Boltzmann formulation is dimensionless. The calculation domain is shown in Fig. 6(a). The 45×90 lattice is employed in the two-dimensional nine-speed lattice-Boltzmann model (D2Q9). The periodic boundary condition is set at both vertical sides. Non-slip bounceback boundary condition is set at all liquid–solid interfaces. The effect of gravity is modeled through a body force acting on the bubble phase.

It should be noted that in practice bubbles are three-dimensional subjects and bubble–liquid interface experiences complex motion at different wavelengths. The present simulation is, however, limited to two-dimensional formulation, neglecting any development of three-dimensional interfacial structures and short waves. It is based on observation of rather symmetrical and quasi-static behavior of bubble during its growth and departure from a nozzle on horizontal surfaces. The situation is less apparent in case of vertical surfaces.

Thus, we assume that the 2D simulation is sufficient to describe the bubble growth and detachment process and we will utilize the bubble departure diameter as a key parameter for evaluating the performance of the lattice-Boltzmann modeling method employed here. Interestingly, main parametric relations described in Eqs. (15) and (16) for the bubble departure diameter can analytically be derived by considering balance of forces acting on a spherical bubble or two-dimensional circular bubble. Although there is no data for circular bubbles, similarity of forces acting on the spherical bubbles and imaginary circular bubbles implies that essential features of Eqs. (15) and (16) remain valid for the circular bubbles.

3.1. Effect of the body (gravity) force

Investigation of the effect of the body (gravity) force

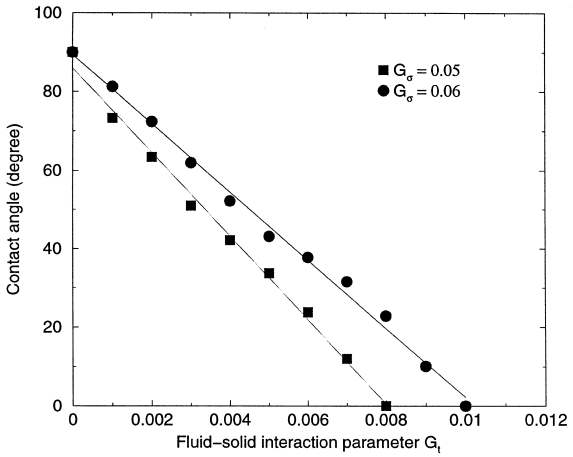

Fig. 5. Evaluation of contact angle of two-phase flow in a pool.

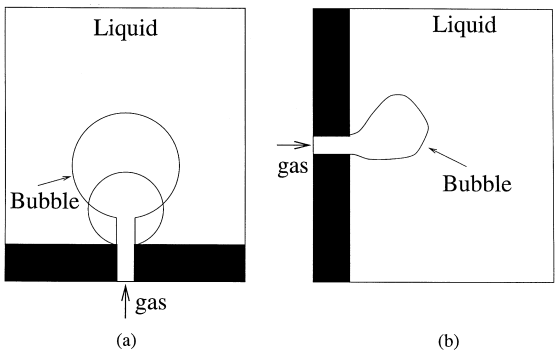

Fig. 6. Calculation domain and schematic of bubble growth, for the horizontal surface (a) and for the vertical surface (b).

on the bubble growth and detachment has recently received significant attention owing to the emerging interest in boiling heat transfer in microgravity conditions. In the literature, it was established that the bubble's departure diameter is proportional to the inverse square root of the gravitational acceleration coefficient $D \sim g^{-1/2}$ (see Eqs. (15) and (16)). However, most of the related experiments were terrestrial. It is therefore of interest to evaluate this dependence for a large variation range of the gravity coefficient. Fig. 7 depicts lattice-Boltzmann simulation results. The bubble's departure diameter calculated for different gravity forces was fit into a function of $D \sim g^{-0.514}$. This result is in very good agreement with the previous theoretical and experimental correlations. Notably, at low gravity conditions, very large departure diameters were predicted. This situation was known to result in an earlier horizontal bubble coalescence and boiling regime transition (boiling crisis). It should also be noted that at low gravity conditions, the role of surface tension and wettability on the bubble departure diameter increases.

Figs. 8 and 9 show essentially similar behavior of bubble growth calculated for two different body forces.

3.2. Effect of the surface tension

Fig. 10 depicts results of lattice-Boltzmann simulations for different values of the surface tension coefficient. A regressional function of the calculated bubble's departure diameter depending on the fluid–fluid interaction potential has the form: $D \sim G_{\sigma}^{1/2}$. Recalling results presented in Fig. 4 about the linear relation between the surface tension coefficient σ and the fluid–fluid interaction potential G_{σ}, it can be concluded that the lattice-Boltzmann method employed is able to predict the well-known relation $D \sim \sigma^{1/2}$. The bubble departure diameter is thus smaller at elevated pressures since the surface tension is associated with the density gradient over the interface of contacting fluids.

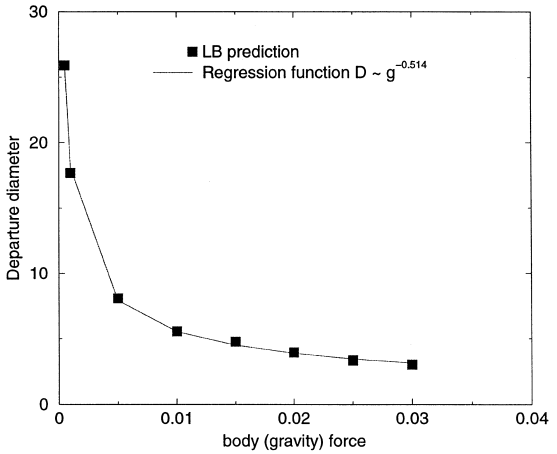

Fig. 7. The body (gravity) force effect on bubble departure diameter, $G_{\sigma} = 0.06$, $G_{\mathrm{t}} = 0.005$, $v = 0.1$.

3.3. Effect of the fluid wettability

The fluid wettability on a solid surface is a nanoscopic phenomenon, which has usually been quantified, macroscopically, in terms of static contact angle at the triple fluid–fluid–solid joining point. In the lattice-Boltzmann modeling, the wettability is implemented through the fluid-solid interaction potential G_{t}. Fig. 11 shows the linear dependence of the bubble's departure diameter on the fluid–solid interaction potential, $D \sim G_{\mathrm{t}}$. Taking into account the calculated results presented in Fig. 5, it can be concluded that the lattice-Boltzmann method is able to describe the linear relation between the bubble departure diameter and the static contact angle as previously established in experiments ($D \sim \beta$).

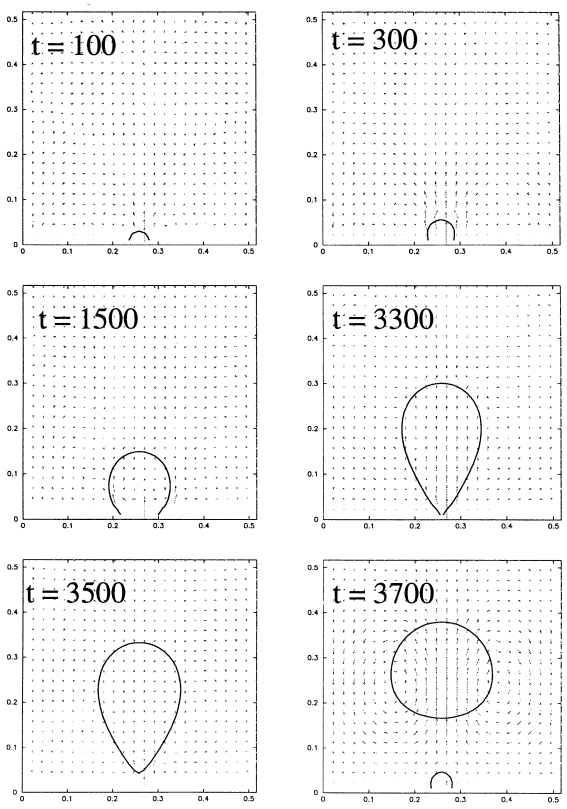

Fig. 8. History of bubble growth and detachment for relatively low body (gravity) force, $G_{\sigma} = 0.06$, $g = 0.001$, $Q = 0.125$, $G_{\mathrm{t}} = 0.005$.

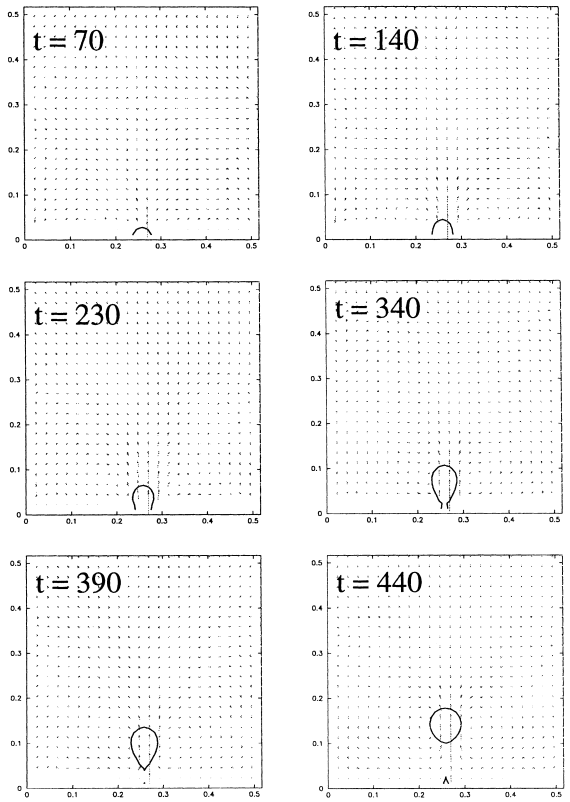

Fig. 9. History of bubble growth and detachment for relatively high body (gravity) force, $G_\sigma = 0.06$, $g = 0.01$, $Q = 0.156$, $G_t = 0.005$.

It is interesting to note that in a nanoscopic neighbourhood around the triple point, the contact angle may well be static. However, with respect to the length scale of the simulation grid size and of currently visualized observations, the contact angle β should, likely, be treated as dynamic due to the effect of the interface inertia on the force balance at the triple point. In certain practical situations, the bubble growth dynamics may be sufficient to necessitate the consideration of the dynamic contact angle. On one hand, such an effect becomes important when the bubble size approaches its departure condition. On the other hand, the bubble growth rate decreases when the bubble volume increases and approaches its departure limit. It is therefore of interest to evaluate the effect of gas flow rate Q on the bubble's departure characteristic.

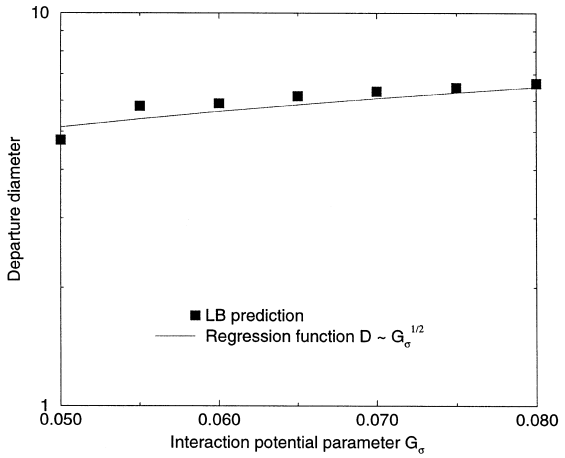

Fig. 10. Surface tension effect on bubble departure diameter, $g = 0.01$, $v = 0.1$, $G_t = 0.005$.

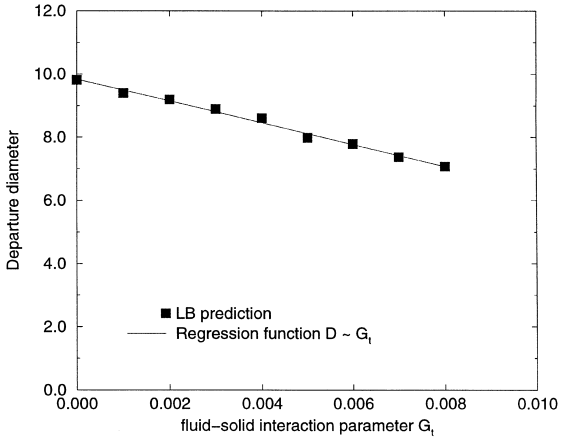

Fig. 11. Wettability effect on bubble departure diameter, $g = 0.01$, $v = 0.1$, $G_\sigma = 0.06$.

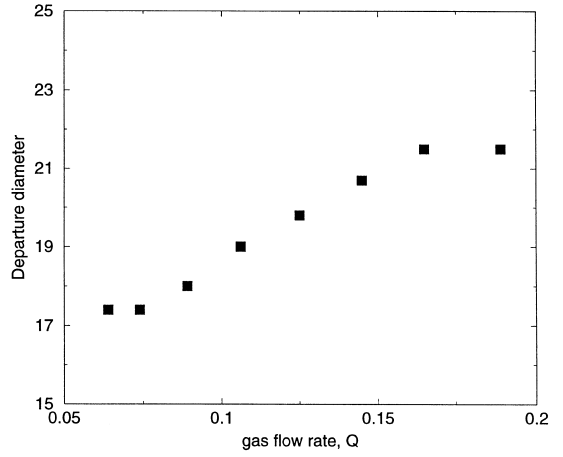

Fig. 12. Flow rate effect on bubble departure diameter for relatively low body (gravity) force, $G_\sigma = 0.06$, $g = 0.001$, $G_t = 0.005$.

3.4. Effect of gas flow rate

Figs. 12 and 13 show the bubble departure diameter calculated for two values ($g = 0.001$ and 0.01) of body force. The dependence of the departure diameter on the flow rate Q can be seen in both cases. In the intermediate range (Q = 0.1–0.2), the effect of the gas flow rate (Q = 0.1–0.2) on the bubble departure diameter is profound and can be evaluated, approximately, as $D \sim Q^{1/3}$ or $D \sim \partial D/\partial t$. This is in reasonably good agreement with experimental data obtained in the past on bubble departure diameter in a large range of gas injection rates. On one hand, it can be stated that such a dependence reflects the correction required for the contact angle under the influence of bubble growth inertia. On the other hand, it may simply indicate the need to consider the dynamic effect of the fast bubble growth on the force balance at the time of the bubble's departure.

As it was noted in Section 1, the present study focuses on the dynamic bubbling regime. However, it might be interesting to make a few notes on results obtained for high and low gas flow rates (turbulent and static bubbling regimes). It was predicted that at both very low and very high gas flow rates, the bubble departure diameter appears to feature another dependence on the gas flow rate. At high gas flow rates, the gas injection regime may well be in jet mode, when surface tension governs the stability and breakup of the jet stream. Therefore, the bubble departure diameter remains constant for a range of the gas flow rate. At small gas flow rates, the bubble's growth inertia can be considered as negligible. However, the dependence of the bubble departure diameter on the gas flow rate was found to differ for different values of body force (g = 0.001 and 0.01). If the static bubbling regime at different gravity conditions would be of interest, a detailed simulation study and comparison to experimental data, in this regime, could be desirable.

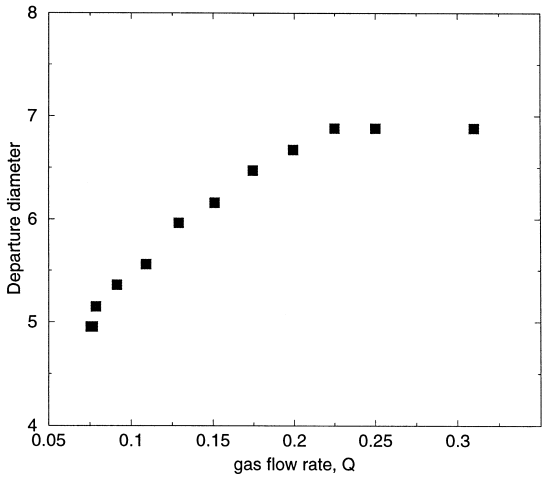

Fig. 13. Flow rate effect on bubble departure diameter under relatively high body (gravity) force, $G_\sigma = 0.06$, $g = 0.01$, $G_t = 0.005$.

4. Bubble growth and detachment on the vertical surface

Interest in the phenomena of bubble growth and detachment on vertical surfaces is largely related to understanding of nucleate boiling and boiling regime transitions. The latter processes are important in many technologies, involving cooling of heated surfaces by a volatile liquid. The bubble growth and detachment have, therefore, been investigated in the context of nucleation and coalescence of vapor bubbles in both pool and flow boiling regimes. The authors are, however, unaware of any separate effect study, in which the isothermal processes of bubble growth and detachment on vertical surfaces were investigated in depth. It remains unclear that how, and to what extent, the different forces acting on the gas bubble alter the beha-

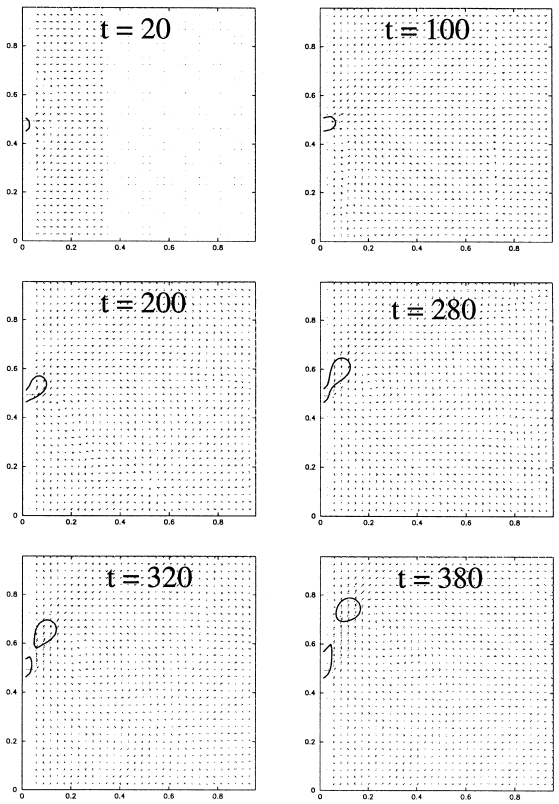

Fig. 14. History of growth and detachment of bubble on a vertical surface, $G_\sigma = 0.06$, $g = 0.01$, $Q = 0.21$, $G_t = 0.01$.

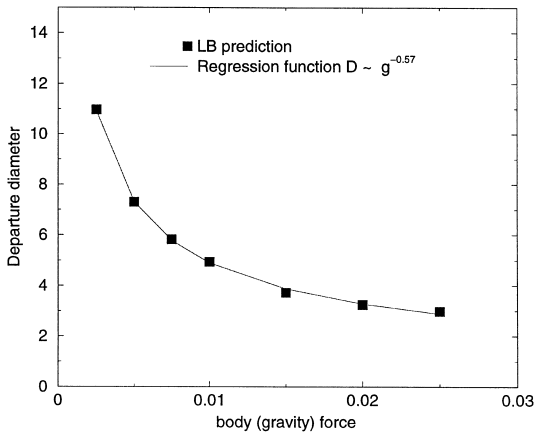

Fig. 15. The body force (gravity) effect on bubble departure diameter, $G_\sigma = 0.06$, $G_t = 0.008$, $v = 0.1$.

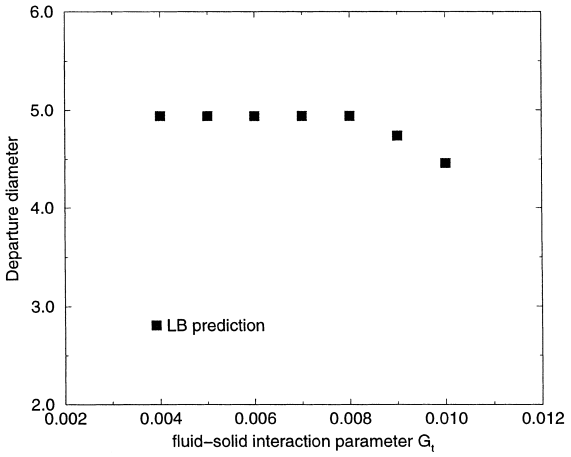

Fig. 17. Wettability effect on bubble departure diameter, $g = 0.01$, $v = 0.1$, $G_\sigma = 0.06$.

vior and characteristics of the bubble growth and detachment on the vertical surfaces, compared to that of the bubbles on the horizontal surfaces.

In the present study, a 70×65 lattice is employed for the computational domain as shown in Fig. 6(b). Periodic boundary conditions are provided for the upper and lower boundaries of the domain. The non-slip condition is assumed on both side vertical boundaries (walls). The FlowLab code is employed for simulation. Qualitative results of the lattice-Boltzmann simulation are depicted in Fig. 14. It can be seen that the bubble growth, detachment and rising on the vertical surface are different from those on the horizontal surfaces. In particular, the bubble shape is not circular (spherical). Actually, the process is asymmetric with respect to the bubble itself. The symmetric circular shape of the bubble simulated is achieved only when it has moved up far enough from the detachment location.

Quantitatively, results of lattice-Boltzmann simulation of the bubble growth and detachment are analyzed in terms of the bubble departure diameter. The effect of the body force (gravity), surface tension, wettability and gas flow rate was numerically investigated. Figs. 15–18 show the dependencies of the bubble departure diameter on the physical parameters and properties chosen.

It can be seen from Fig. 15 that the body force (gravity) imposes a significant effect on the bubble departure diameter, $D \sim g^{-0.57}$. The power index 0.57

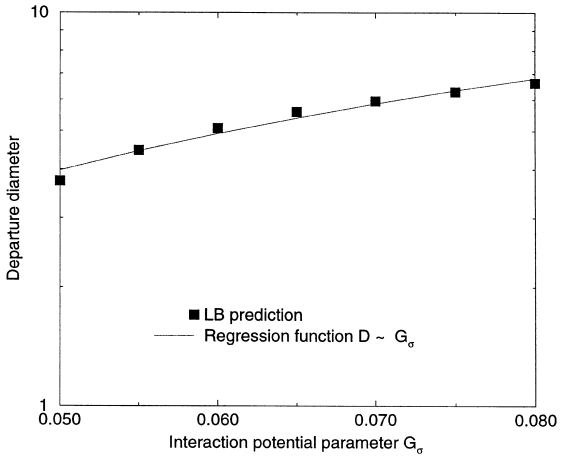

Fig. 16. Surface tension effect on bubble departure diameter, $g = 0.01$, $v = 0.1$, $G_t = 0.006$.

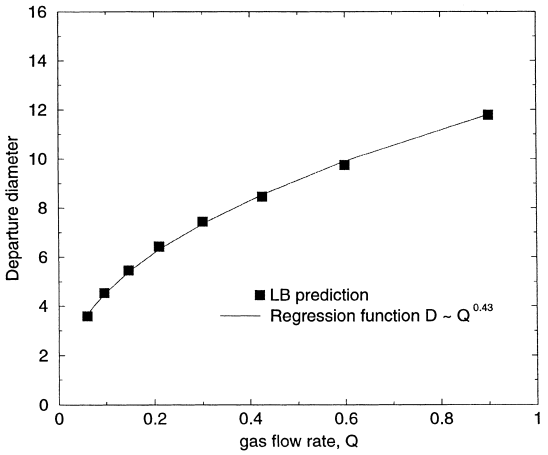

Fig. 18. Flow rate effect on bubble departure diameter, $G_\sigma = 0.06$, $g = 0.01$, $G_t = 0.01$.

resulted from a regression analysis is higher than the power index of 0.514, which was obtained for the departure diameter of the bubble on the horizontal surface.

Fig. 16 shows a linear dependence of the bubble's departure diameter on the surface tension coefficient, $D \sim G_\sigma \sim \sigma$. Such a dependence is stronger than that observed and predicted for the bubble's departure diameter on the horizontal surfaces ($D \sim G_\sigma^{1/2} \sim \sigma^{1/2}$). It is perhaps, related to the effect of surface tension in the neck region of the bubble interface near the detachment location. This force acts either perpendicular or parallel to the direction of the bubble moving from horizontal or vertical surfaces, respectively.

Fig. 17 shows the effect of wettability on the bubble's departure diameter for the vertical surface case. It was found that when both fluids feature good wettability characteristics, the bubble's departure diameter is not affected by the wettability. However, when the bubble phase becomes less wettable, the bubble's departure diameter is predicted to decrease as it was also observed in the case of bubble departure from the horizontal surfaces.

Fig. 18 shows the effect of gas flow rate on the bubble's departure diameter. Interestingly, no saturation regime was predicted at both low and high gas flow rates, indicating specificity of the horizontal injection of gas through a nozzle on the vertical surface.

Finally, it should be noted that analytical modeling of the bubble departure on the vertical surface is difficult due to the bubble's asymmetry. The above results of lattice-Boltzmann simulation have yet to be verified against experimental data. Nonetheless, the dependencies predicted by lattice-Boltzmann simulation provide useful insight in developing understanding and an appropriate analytical model.

5. Conclusions

In the present work, the FlowLab code, based on the D2Q9 lattice-Boltzmann model for two-phase flow is employed to simulate the behavior of bubble growth and detachment from a nozzle on the horizontal and vertical surfaces.

To enable studying separate effects in the bubble growth and detachment phenomena, conditions were chosen to cope with the current limitations of the lattice-Boltzmann technique in handling fluid pairs with significant differences in physical properties. It was found that the approach provides a realistic picture of the bubble behavior. More importantly, analysis of the lattice-Boltzmann simulation results revealed that the major parametric dependencies of the bubble's departure diameter on various physical parameters (body force, gas generation rate) and physical properties (surface tension, wettability) are correctly predicted. In particular, the lattice-Boltzmann simulation results were found to be in excellent agreement with experimentally established dependencies of the departure diameter of bubbles on the horizontal surfaces. The simulation results obtained for bubbles on vertical surfaces also provide useful insights into the phenomena of bubble growth and detachment.

It should be noted that the present work was performed to explore the capabilities and limitations of the lattice-Boltzmann method, in general, and the FlowLab code, in particular, for multiphase-flow modeling. The optimistic results of the present study serve as the starting point for continued studies on bubble coalescence and boiling regime transitions through the lattice-Boltzmann method.

References

[1] D.J. McCann, R.G. Prince, Regimes of bubbling at a submerged orifice, Chemical Engineering Science 26 (1971) 1505–1512.
[2] Yu.A. Buyevich, V.V. Butkov, On the mechanism of bubble formation at gas flow into liquid through a circular orifice, Theor. Osn. Khim. Tekh. (in Russian) 5 (1971) 74–83.
[3] A. Marmur, E. Rubin, Equilibrium shapes and quasi-static formation of bubbles at submerged orifice, Chemical Engineering Science 28 (1973) 1455–1464.
[4] Yu.A. Buyevich, B.W. Webbon, Bubble formation at a submerged orifice in reduced gravity, Chemical Engineering Science 51 (1996) 4843–4857.
[5] A.E. Wraith, Two stage bubble growth at a submerged plate orifice, Chemical Engineering Science 26 (1971) 1659–1671.
[6] J.F. Davidson, B.O. Schuler, Bubble formation at an orifice in a viscous liquid, Transactions Institute of Chemical Engineers 38 (1960) 144–154.
[7] J.F. Davidson, B.O. Schuler, Bubble formation at an orifice in an inviscous liquid, Transactions Institute of Chemical Engineers 38 (1960) 342–355.
[8] J.K. Walters, J.F. Davidson, The initial motion of a gas bubble formed in an inviscid liquid, Part 2. The three-dimensional bubble and the toroidal bubble, Journal of Fluid Mechanics 17 (1963) 321–336.
[9] Y.H. Qian, D. D'Humieres, P. Lallemand, Lattice BGK models for Navier–Stokes equation, Europhysics Letters 17 (1992) 479–484.
[10] Z.L. Yang, R.R. Nourgaliev, T.N. Dinh, B.R. Sehgal, Investigation of two-phase flow characteristics in a debris particle bed by a lattice-Boltzmann model, in: Second International Symposium on Two-Phase Flow Modeling and Experimentation, Pisa, Italy, May 23–25, 1999.
[11] R.R. Nourgaliev, T.N. Dinh, B.R. Sehgal, Numerical simulation of droplet deformation and break-up by a lattice-Boltzmann method, in: CD-ROM Proceedings of

the Third International Conference on Multiphase Flow, Lyon, France, June 8–12, 1998.
[12] X. Shan, H. Chen, Lattice-Boltzmann model for simulating flows with multiple phases and components, Physical Review E 47 (1993) 1815–1819.
[13] X. Shan, G. Doolen, Diffusion in a multicomponent lattice-Boltzmann equation model, Physical Review E 54 (1996) 3614–3620.
[14] N.S. Martys, H. Chen, Simulation of multi-component fluids in complex three-dimensional geometries by the lattice-Boltzmann method, Physical Review E 53 (1996) 743–750.
[15] R.S. Maier, R.S. Bernard, Accuracy of the lattice-Boltzmann method, International Journal of Modern Physics C 8 (4) (1997) 747–752.
[16] W. Fritz, Maximum volume of vapor bubbles, Physik Zeitschr. 36 (1935) 379–384.
[17] B.E. Staniszewski, Nucleate boiling bubble growth and departure, MIT Tech. Rep. No. 16, Division of Sponsored Research, Cambridge, MA, 1959.